Numerical simulations of light scattering by red blood cells

Karlsson, Anders; He, Jiangping; Swartling, Johannes; Andersson-Engels, Stefan

Published in:
IEEE Transactions on Biomedical Engineering

DOI:
10.1109/TBME.2004.839634

2005

Numerical Simulations of Light Scattering by Red Blood Cells

Anders Karlsson*, Jiangping He, Johannes Swartling, and Stefan Andersson-Engels

***Abstract*—Scattering of electromagnetic waves from a red blood cell is simulated using the finite-difference time-domain method (FDTD), the Rytov approximation and the discrete dipole approximation (DDA). Both FDTD and DDA are full wave methods that give accurate results in a wide range of wavelengths. The Rytov approximation is a much simpler method that is limited to scattering angles within 30° from the forward direction. The investigation comprehends different wavelengths and different orientations of the cell. It shows that the shape, volume, and orientation of the cell have a large influence on the forward scattering.**

***Index Terms*—Biological tissues, blood, optical propagation in nonhomogeneous media, optical scattering.**

I. Introduction

LIGHT scattering properties of tissue are important for many medical applications. It has an influence on dosimetry of laser therapy [11], [13], [15], light scattering spectroscopy [4], [5], [18], and optical analysis of blood for blood related diseases. For all these applications the properties of the blood play an important role. These important applications, thus, motivate efforts in improving experiments, theory, and numerical simulations in blood optics. This paper focuses on the numerical simulations. The size of a red blood cell (RBC) is typically 5–10 wavelengths in the optical region and at a vacuum wavelength of 630 nm, the values for the index of refraction is 1.40 for a blood cell and 1.35 for the plasma. From a computational point of view this is a very large, but weakly scattering object. The weak scattering enables a modern computer to make accurate simulations with execution times less than an hour and with an allocation of less than 500-Mbyte RAM. Three different methods for simulations of scattering from a nonspherical RBC are used in the paper. The accurate calculations by a finite-difference time-domain method (FDTD) are compared with calculations from the Rytov approximation and the discrete dipole approximation (DDA). The methods agree surprisingly well for a realistic RBC model. In particular, DDA is as accurate as FDTD, but turns out to be faster and less memory requiring.

Manuscript received August 20, 2003; revised May 9, 2004. This work was supported in part by the Swedish Research Council. *Asterisk indicates corresponding author.*

*A. Karlsson is with the Department of Electroscience, Lund University, Lund 221 00, Sweden (e-mail: anders.karlsson@es.lth.se).

J. He is with the Department of Electroscience, Lund University, Lund 221 00, Sweden.

J. Swartling and S. Andersson-Engels are with the Department of Physics, Lund University, Lund 221 00, Sweden.

Digital Object Identifier 10.1109/TBME.2004.839634

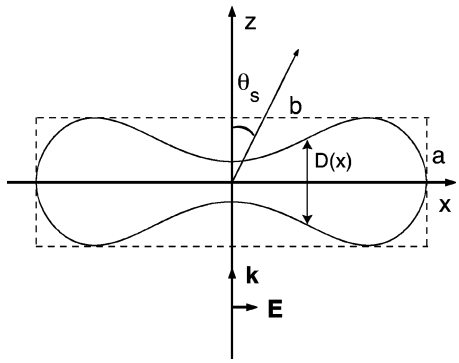

Fig. 1. RBC cross section for simulations $a = 2.55\ \mu\mathrm{m}$ and $b = 7.76\ \mu\mathrm{m}$.

It is well known that RBCs, *in vivo* or *in vitro*, display a number of different shapes [3]. In general, the normal RBC shape is a discocyte, i.e., an axially symmetric disc, slightly indented on the axis. The information from simulations from such realistic shapes are useful in the development of models of light propagation in whole blood containing many RBCs. A number of such simulations were performed for different shapes, wavelengths, and angles of incidence.

The basic definitions and physical parameters are given in the next section. This is followed by a discussion of the three methods in Section III. The numerical results are presented and discussed in Section IV, and some concluding remarks are given in the last section.

II. Preliminaries

In the simulations, the refractive index of the RBC is set to $n_1 = 1.406$ and the refractive index of the surrounding blood plasma is set to $n_2 = 1.345$. The relative index of refraction, defined by n_1/n_2, is then 1.045. All wavelengths refer to vacuum. Absorption can be handled by the numerical methods employed in the paper, but for the wavelengths used in the simulations it is small and has been neglected. Graphs presented in cf. [9] show that the absorption coefficient μ_a is less than 5 mm^{-1} at 630 nm. The model of the disc-like RBC that is used in the simulations is defined in [10], and Fig. 1 shows the corresponding cross section. The explicit expression for the thickness $D(x)$ reads

$$D(x) = \sqrt{1 - \left(\frac{x}{R_0}\right)^2}\left[C_0 + C_2\left(\frac{x}{R_0}\right)^2 + C_4\left(\frac{x}{R_0}\right)^4\right] \tag{1}$$

where $R_0 = 3.91\ \mu\mathrm{m}$, $C_0 = 0.81\ \mu\mathrm{m}$, $C_2 = 7.83\ \mu\mathrm{m}$, and $C_4 = -4.39\ \mu\mathrm{m}$, which corresponds to a volume of 94 $\mu\mathrm{m}^3$.

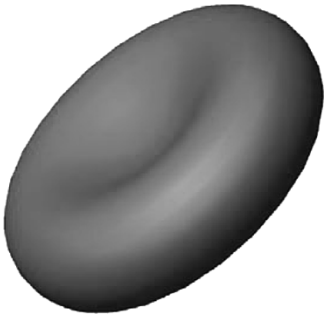

Fig. 2. Three-dimensional RBC.

The three-dimensional (3-D) shape, depicted in Fig. 2, is obtained by rotating the cross section around the z-axis. The membrane of an RBC has a negligible influence on the scattered field, cf. [16] and [17] and hence the RBC models do not include the membrane or any other internal structure. The incident wave is a time-harmonic linearly polarized plane wave. It propagates in the positive z-direction with the electric field in the x-direction. With the time convention $e^{-i\omega t}$, the complex incident electric field is given by

$$\vec{E}_{\text{inc}}(z) = \hat{x} E_0 e^{ikz} \tag{2}$$

where $k = n_2\omega/c_0$ is the wave number for the plasma and c_0 is the velocity of light in vacuum. The angle of incidence is altered by rotating the RBC around the y-direction. The rotation angle of the axis of symmetry relative the z-direction is denoted θ_i. Fig. 1 shows the case when $\theta_i = 0^\circ$. To interrelate the angular distributions of the scattered light of different incident wavelengths and angles, the scattering probability is calculated as a function of the zenith scattering angle θ_s (see Fig. 1) This scattering probability, $P(\theta_s)$, is obtained by numerical integration of the differential scattering cross section, $\sigma_{\text{diff}}(\theta_s, \phi_s)$, over all azimuthal angles $\phi_s \in [0, 2\pi]$

$$P(\theta_s) = \frac{\int_0^{2\pi} \sigma_{\text{diff}}(\theta_s, \phi) \sin\theta_s d\phi}{\int_0^{2\pi}\int_0^{\pi} \sigma_{\text{diff}}(\theta, \phi) \sin\theta d\theta d\phi}. \tag{3}$$

Thus, $P(\theta_s)d\theta_s$ is the probability that a scattered photon is scattered in the theta interval $[\theta_s, \theta_s + d\theta_s]$. Due to the factor $\sin\theta_s$ the probability is zero in the forward direction. The differential cross section is defined by

$$\sigma_{\text{diff}}(\theta, \phi) = r^2 \frac{\left\langle \vec{S}(r, \theta, \phi) \cdot \hat{r} \right\rangle}{\langle \vec{S}_{\text{inc}} \cdot \hat{z} \rangle} \tag{4}$$

where

$$\begin{aligned} \left\langle \vec{S}_s(r, \theta, \phi) \right\rangle &= \frac{1}{2}\text{Re}\left\{ \vec{E}(r, \theta, \phi) \times \vec{H}^*(r, \theta, \phi) \right\} \\ \langle \vec{S}_{\text{inc}} \rangle &= \frac{1}{2}\text{Re}\left\{ \vec{E}_{\text{inc}}(z) \times \vec{H}^*_{\text{inc}}(z) \right\} \\ &= \frac{1}{2}\frac{n_2}{\eta_0}|E_0|^2 \hat{z} \end{aligned} \tag{5}$$

are the time averages of the Poynting vector of the scattered and incident fields, respectively. Furthermore, $\hat{r}$ is the radial unit vector, $\vec{E}(r, \theta, \phi)$ is the scattered electric field, $\vec{H}^*(r, \theta, \phi)$ is the complex conjugate of the corresponding magnetic field, and $\eta_0 = 120\pi\ \Omega$ is the wave impedance of vacuum. The far-field amplitude, $\vec{F}(\theta, \phi)$, of the scattered field is defined by

$$\lim_{r\to\infty} \vec{E}(r, \theta, \phi) = \vec{F}(\theta, \phi)\frac{e^{ikr}}{kr}. \tag{6}$$

III. Methods

Recently, a number of different numerical methods have been applied to blood optics. A robust method is Mie scattering, where a spherical model of the RBC is used. Comparisons with Mie scattering are very useful tests for numerical methods. The T-matrix method, cf. [19] and [24], is a generalization of Mie scattering. In [19], it was indicated that the T-matrix method is not a suitable method for RBC with realistic shapes. Today FDTD is a very important method for all kinds of electromagnetic wave propagation applications, cf. [20], and it has been used for cell optics, cf. [1], [7], and [8]. The boundary element method (BEM) is also a widely used numerical method in electromagnetics. It is based on a surface integral equation for the electromagnetic fields and was applied to scattering from blood cells in [22], [23].

This section discusses FDTD, DDA, and the Rytov approximation. The first two methods solve the full Maxwell equations, whereas the Rytov approximation is based on the approximation that the RBC is a weakly scattering object. The Rytov approximation requires less than one hundred lines of code and is considerably faster than the other two methods. The drawback is that it is not accurate for large scattering angles.

A. FDTD

The finite difference time domain algorithm was originally applied to the Maxwell equations by Yee in 1966 [25]. A review of recent progresses of the method are given in the book by Taflove [20]. In the 3-D case, the Maxwell curl equations are discretized in time and space, resulting in six coupled scalar finite-difference equations in cartesian coordinates. All three electric field components and all three magnetic components are spatially allocated as in Fig. 3. The electric and magnetic fields are temporally offset and stepped in a leap frog scheme using the finite-difference form of the curl operator. In order to calculate the angular far-field distribution of the scattered light, several techniques are required.

1) **Absorbing boundary condition (ABC)**: The computational domain is finite. With no truncation conditions, the waves are artificially reflected at the boundaries of the domain, leading to inaccurate results. The reflections are avoided by implementing ABC that does not reflect waves. The perfectly matched layer (PML) ABC, suggested by Berenger [2], has been implemented in the 3-D FDTD program. In this paper, the split-type PML is used. In this PML medium, each component of the electromagnetic field is split into two parts. In cartesian coordinates, the six components yield 12 subcomponents denoted as E_{xy}, E_{xz}, E_{yx}, E_{yz}, E_{zx}, E_{zy}, H_{xy}, H_{xz}, H_{yx}, H_{yz}, H_{zx}, and H_{zy}. The Maxwell equations are replaced by

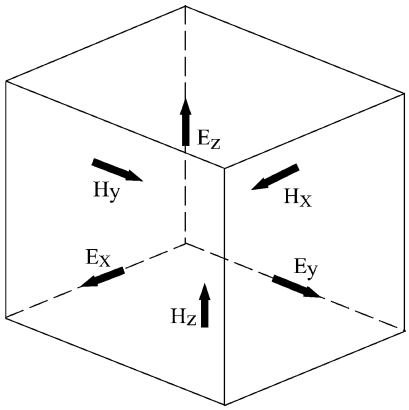

Fig. 3. Unit cell in 3-D FDTD algorithm.

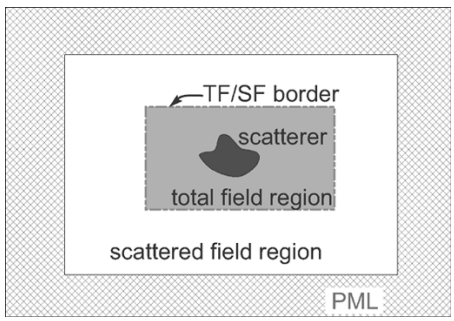

Fig. 4. Total field/scattered field regions.

12 equations. In our simulations, 8 PML layers with reflection coefficient 10^{-8} are chosen. The [2], [20] contain more detailed descriptions of PML.

2) **Total field/scattered field**: Since this work considers the scattering patterns, the total field/scattered field formulation is used. The computational grid is divided into two regions. The total field region encloses the scatterers whereas the scattered field region, where only the scattered field components are stored, encloses the total field region, as illustrated in Fig. 4. At the border between the two regions, special connecting conditions are required, where the incident field is either within, or subtracted from, the total field. The conditions used for the simulations in the paper are described in detail in [20].
3) **Far-Field Transformation**: FDTD is inherently a near-field method. To determine the far-field scattering pattern, the near-field data is transformed to the far-field by the near-field to far-field (NFFF) transformation. The details of the NFFF technique can be found in [20].

B. The Discrete Dipole Approximation (DDA)

The DDA is closely related to the method of moments, cf. [12]. The principle of the method is as follows: The scattering volume is divided into N parts. Each part is small enough to be represented by a dipole moment. Linearity of the medium implies that the induced dipole moment of each volume element is equal to the electric field in the volume multiplied by the polarizability of the volume. The electric field is a superposition of the fields from the sources external to the object and the electric fields from the sources inside the object, in this case the $N-1$ dipoles. The field from the external sources is the incident plane wave and hence the electric field in volume j is given by

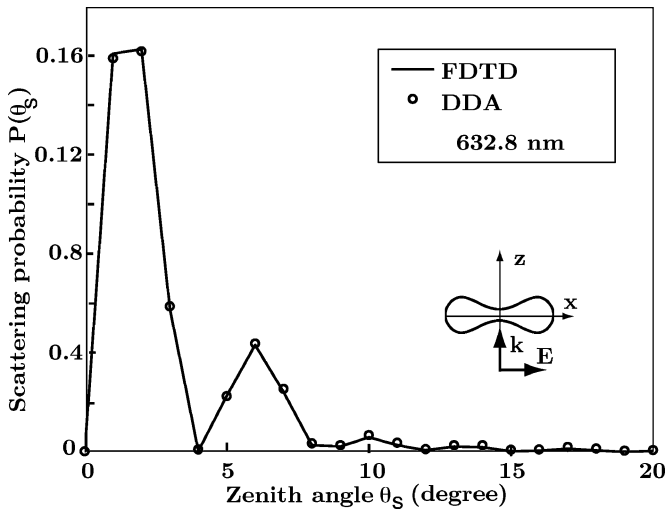

Fig. 5. The scattering probability, cf. (3) for a disc-like RBC using FDTD and DDA. ($\theta_i = 0°$, $\lambda = 632.8$ nm).

$$\vec{E}(\vec{r}_j) = \vec{E}_{\text{inc}}(\vec{r}_j) - \sum_{k \neq j} \mathbf{A}(\vec{r}_j, \vec{r}_k) \cdot \vec{p}(\vec{r}_k). \tag{7}$$

The term $-\mathbf{A}(\vec{r}_j, \vec{r}_k) \cdot \vec{p}(\vec{r}_k)$ is the electric field at a position $\vec{r}_j$ from a dipole at position $\vec{r}_k$. The explicit expressions of the quantities involved in (7) can be found in, e.g., [6]. Equation (7) is usually solved by some iterative method, e.g., the conjugate gradient method. For scattering objects with a relative index of refraction close to one the iteration methods converge very fast. In [6] it is indicated that the DDA method gives rise to erroneous results if the contrast is large, i.e., if $n_1 \gg n_2$, otherwise the method is stable and the error decreases when the size of the numerical cells decreases. In Fig. 5, the scattering probabilities for a disc-like RBC using FDTD and DDA are shown. Both methods are very accurate, but DDA requires less memory and is faster than FDTD. In all of the calculations done in this project, the DDA and the FDTD have given results that agree to a very high accuracy.

C. Superposition

Since the relative index of refraction of the RBC is close to one it is anticipated that for a single RBC the multiple scattering effects are almost negligible. When multiple scattering is neglected, the scattered fields from different parts of the RBC can be added to form the total field, i.e., the superposition principle holds for the scattered field. In the example depicted in Fig. 6 a blood cell was divided in two halves through the yz-plane. The far-field pattern of the electric field was calculated for each half by FDTD in the yz-plane. Then the two far-fields were added and compared with the far-field from the whole blood cell. The patterns agree, except in the directions where the scattered field is very small, as seen from Fig. 6. This emphasizes that multiple scattering effects are small. The superposition approximation facilitates the calculation of far-fields from very large, weakly scattering objects, where it reduces the CPU-time and the required RAM of the computer.

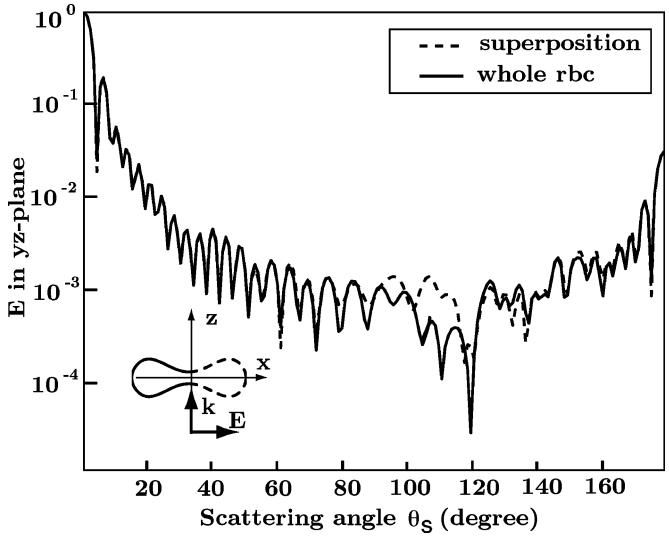

Fig. 6. The normalized scattered electric far-field $|\vec{E}|$ in the yz-plane from an FDTD simulation. The solid line refers to the whole RBC. The dash line is the superposition of the scattered far-field from the left and right halves of the whole RBC. ($\theta_i = 0°$, $\lambda = 632.8$ nm).

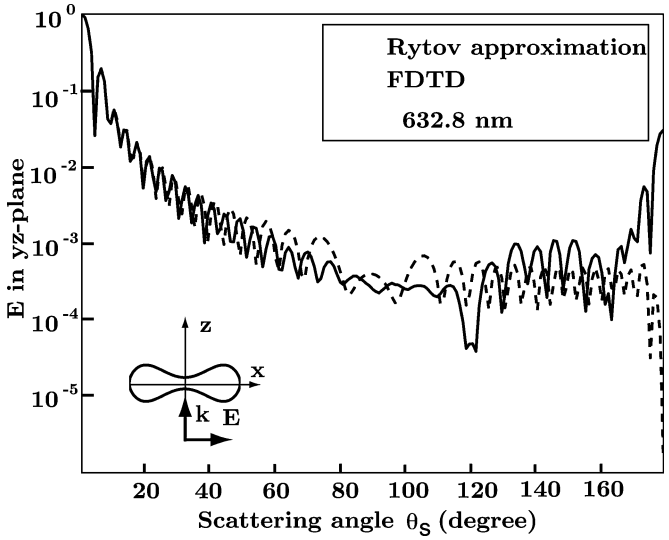

Fig. 7. The normalized scattered far-field $|\vec{E}|$ in the xz-plane by a disc-like RBC using the Rytov approximation and FDTD. ($\theta_i = 0°$, $\lambda = 632.8$ nm).

D. The Rytov Approximation

The Rytov approximation is a frequently used method in tomography, [12], [14], [21]. It is then utilized for the inverse scattering problem of determining the permittivity or conductivity of an object. In this paper, it is applied in its simplest form to the scattering of a plane wave from an RBC. The method can be explained as follows: Consider an object that occupies the volume V. Let the index of refraction be n_1 for the object and n_2 for the surrounding medium. The incident wave is given by (2). The approximation assumes that when the wave passes the object, the phase of the wave is shifted while its amplitude, polarization, and direction of propagation are unaltered. Let $d(x, y)$ be the total distance the ray travels inside the scattering object. If $z = z_1$ is a plane behind the object, the total electric field in that plane reads

$$\vec{E}(x, y, z_1) = \hat{x} E_0 e^{ik_0(n_2 z_1 + (n_1 - n_2)d(x,y))}. \quad (8)$$

Thus, the phase is shifted an angle $k_0(n_1 - n_2)d(x, y)$, compared to the incident wave. The far-field amplitude, cf. (6), is given by the near-field to far-field transformation, cf. [20], i.e.,

$$\vec{F}(\theta, \phi) = i\frac{k^2}{4\pi} E_0 e^{ikz_1} \left(\hat{r} \times \iint_S (\hat{y} - \hat{r} \times \hat{x}) \right) \times \left(e^{ik_0(n_1 - n_2)d(x,y)} - 1 \right) e^{-ik\hat{r}\cdot\vec{r}} \mathrm{d}x\mathrm{d}y \quad (9)$$

where S is the plane $z = z_1$. Notice that the integrand is zero outside the projection of the blood cell on the plane $z = z_1$. The Rytov approximation ignores multiple scattering as well as backscattering. Consequently, it is an even more approximate method than the superposition method. Since the reflected waves are neglected, the method is limited to scattering angles $\theta_s < \pi/2$. In practice this interval is smaller, the calculated far-field pattern is quite accurate for scattering angles less than $\pi/6$, as can be seen in Fig. 7, but for larger angles the errors are not acceptable. The code for Rytov approximation and the transformation to the far-field amplitude is very short and simple. The calculation of the far-field pattern is done in a couple of seconds.

IV. Results and Discussion

The simulations show that FDTD and DDA are both very accurate for scattering from one RBC. The errors in the numerical calculations can be estimated by comparing results using two different grid sizes. Such error tests confirm that the graphs presented for FDTD and DDA are correct. Both methods have also been compared with Mie scattering from a sphere with excellent agreement.

The RBC has a relative refractive index close to one and its surface is slowly varying compared to the wavelength. Both FDTD and DDA benefit from these two properties. The smooth surface ensures that the grid size is determined by the wavelength and not by the geometry, and this keeps the allocated RAM at a minimum. The low relative refractive index implies that there are no pronounced resonances in the object and the execution times are then proportionally short.

Today FDTD is one of the most powerful full wave methods available. In a number of papers it has proven to be suitable for blood optics. However, the results in this paper indicate that it is not the most efficient method. The DDA is faster than FDTD, it requires less RAM and gives results that are as accurate as FDTD. The DDA is closely related to the method of moments. The difference is that the method of moments is derived from a volume integral equation. It is expected that the method of moments should also be a suitable method for blood analysis. The BEM is similar to the method of moments but is based on a surface integral equation. The BEM has successfully been applied to blood optics, cf. [22] and [23]. In [23] scattering from aggregated blood cells was analyzed. The geometry was axially symmetric, and that symmetry was utilized to reduce the execution time.

The Rytov approximation simplifies the problem since it only considers the phase shift of the incident plane wave. Nevertheless, it gives remarkably accurate values for scattering angles up

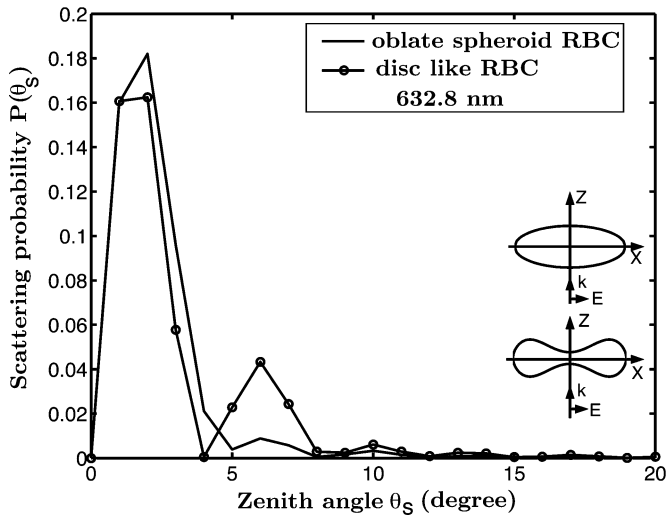

Fig. 8. The scattering probability, cf. (3) for an oblate spheroid with semi-axes 1.47 μm and 3.91 μm, and a disc-like RBC with the same volume. ($\theta_i = 0°$, $\lambda = 632.8$ nm).

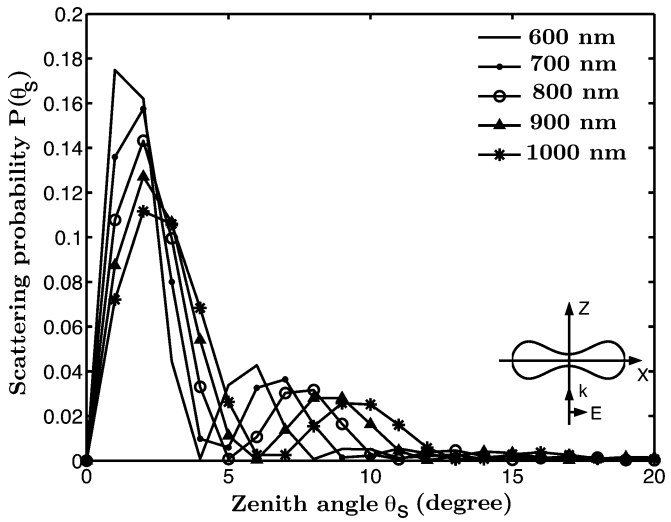

Fig. 9. The scattering probability, cf. (3) for a disc-like RBC excited by an incident plane wave, at five different wavelengths. The angle of incidence is $\theta_i = 0°$.

to roughly $\pi/6$. The results indicate that it should be possible to develop fast, but robust, approximate methods that can handle scattering from a large number of RBC.

The comparison of different numerical methods was one of the two objectives of the paper. The other was to investigate the scattering properties of an RBC. The main purpose with most of the graphs is to examine the influences the shape and orientation of the RBC have on the scattered field. The simulation program *SEMCAD* (see www.semcad.com), which is an FDTD program, was used for the simulations of the far-field scattering pattern. However, one could just as well have used DDA. In all the FDTD simulation cases, the grid space was adaptively set between $\lambda/10$ and $\lambda/20$ in order to yield accurate results.

A. Shape of the RBC

The influence the shape of the RBC has on the scattering pattern was investigated by a comparison of the patterns for the oblate spheroidal RBC and the disc-like RBC in Fig. 1. The two RBC have equal volume and material parameters. The vacuum wavelength is 632.8 nm and the incident angle θ_i is 0°. Fig. 8 shows that the shape of the RBC has a significant influence on the scattering pattern for small scattering angles. The second peak in the pattern for the disc-like shape is due to the interference of the fields from the two thick parts of the cross section. The position of the second peak appears approximately where there is a 2π phase difference between the far-fields from the two parts. The angle for the peak is approximately given by

$$\theta_s = \arcsin\left(\frac{\lambda}{(n_1 d)}\right) \tag{10}$$

where d is the distance between the thick parts. The estimated value $d = 4.5$ μm gives almost a correct angle for the second peak.

B. Wavelength and Angle of Incidence

Accurate simulations of the scattering from the disc-like RBC in Fig. 1 were conducted by FDTD for the three angles of incidence 0°, 45°, 90°. For each of the incident angles five wavelengths from 600 nm to 1000 nm are used.

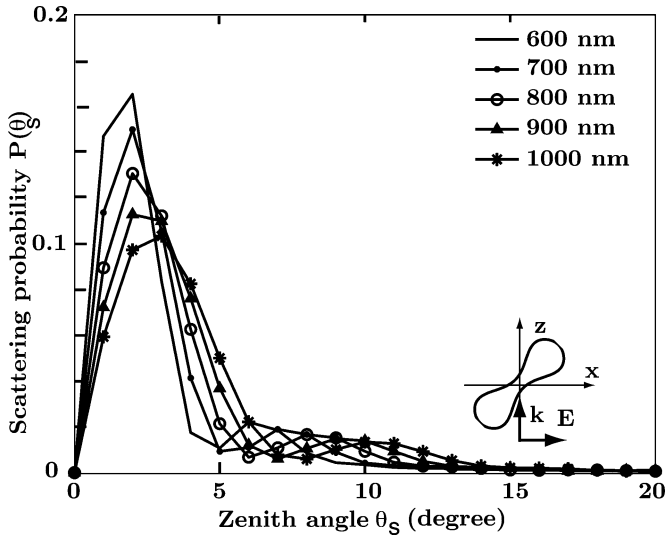

Fig. 10. The same cases as in Figs. 9 and 11 and but for an incident angle of $\theta_i = 45°$.

Fig. 9 demonstrates that the incident wavelength has a strong influence on the scattering pattern for $\theta_i = 0$. The forward scattering is strong and, as in Fig. 8, the second peak is due to the constructive interference between two fields where the angle for the second peak is approximately given by (10).

The scattering pattern for the 45° case is depicted in Fig. 10. The peaks in the forward direction are similar to the corresponding peaks in the 0° case, for each wavelength. However, the second peak is much less pronounced.

The scattering patterns for $\theta_i = 90$ differ from the patterns for the other two incident angles. This is due to the lack of interference and to the averaging over the azimuthal angle.

V. Conclusion

In this paper, FDTD, DDA, and the Rytov approximation were applied to scattering from a single RBC. Both FDTD and DDA give accurate far-field patterns. Even though FDTD today

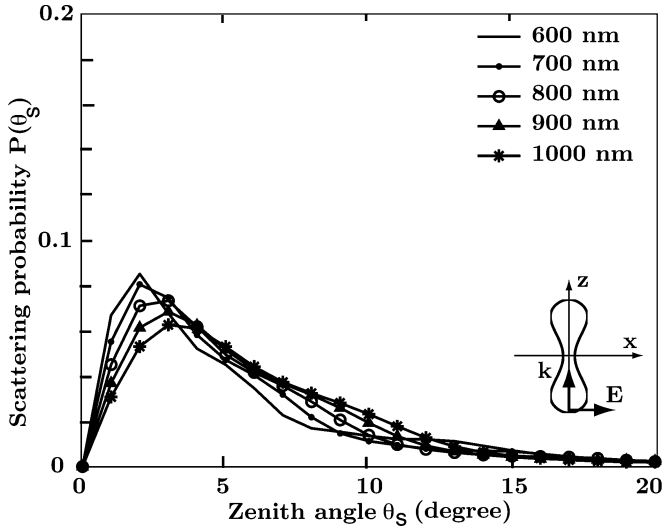

Fig. 11. The same cases as in Figs. 9 and 10 but for an incident angle of $\theta_i = 90^\circ$.

is a more frequently used method in blood optics the results indicate that there are frequency domain methods, e.g., the DDA method, that are more suitable. In order to develop a fast but yet accurate method that can simulate the propagation of light in samples with a large number of blood cells one has to utilize the fact that the relative index of refraction for the RBC is close to one. The simulations using the DDA method, the Rytov approximation, and superposition support that conjecture.

REFERENCES

[1] D. Arifler *et al.*, "Light scattering from normal and dysplastic cervical cells at different epithelial depths: finite-difference time-domain modeling with a perfectly matched layer boundary condition," *J. Biomed. Opt.*, vol. 8, pp. 484–494, 2003.

[2] J. P. Berenger, "A perfectly matched layer for the absorption of electromagnetic waves," *J. Computational Phys.*, vol. 114, pp. 185–200, 1994.

[3] M. Bessis, "Red cell shapes: an illustrated classification and its rationale," *Nouv. Rev. Fr. Hematol.*, vol. 12, pp. 721–746, 1972.

[4] I. J. Bigio *et al.*, "Diagnosis of breast cancer using elastic-scattering spectroscopy: preliminary clinical results," *J. Biomed. Opt.*, vol. 5, pp. 221–228, 2000.

[5] I. J. Bigio, J. R. Mourant, and G. Los, "Noninvasive, in-situ measurement of drug concentrations in tissue using optical spectroscopy," *J. Gravit. Physiol.*, vol. 6, pp. 173–175, 1999.

[6] B. T. Draine and P. J. Flatau, "Discrete-dipole approximation for scattering calculations," *J. Opt. Soc. Am. A*, vol. 11, no. 4, pp. 1491–1499, 1994.

[7] R. Drezek, A. Dunn, and R. Richards-Kortum, "Light scattering from cells: finite-different time-domain simulations and goniometric measurements," *Appl. Opt.*, vol. 38, no. 16, pp. 3651–3661, 1999.

[8] A. Dunn *et al.*, "Finite-difference time-domain simulation of light scattering from single cells," *J. Biomed. Opt.*, vol. 2, no. 3, pp. 262–266, 1997.

[9] A. M. K. Enejder, "Light Scattering and Absorption in Tissue-Models and Measurements," Ph.D. thesis, Lund Institute of Technology, Lund, Sweden, 1997.

[10] E. Evans and Y. Fung, "Improved measurement of the erythrocyte geometry," *Microvasc. Res.*, vol. 4, pp. 335–347, 1972.

[11] S. Iinuma *et al.*, "In vivo fluence rate and fractionation effects on tumor response and photobleaching: photodynamic therapy with two photosensitizers in an orthotopic rat tumor model," *Cancer Res.*, vol. 59, pp. 6164–6170, 1999.

[12] A. Ishimaru, *Electromagnetic Wave Propagation, Radiation, and Scattering*. Englewood Cliffs, NJ: Prentice-Hall, Inc., 1991.

[13] T. Johansson *et al.*, "Feasibility study of a novel system for combined light dosimetry and interstitial photodynamic treatment of massive tumors," *Appl. Opt.*, vol. 41, pp. 1462–1468, 2002.

[14] A. C. Kak and M. Slaney, *Principles of Computerized Tomographic Imaging*. Piscataway, NJ: IEEE Press, 1988.

[15] L. Lilge, K. Molpus, T. Hasan, and B. C. Wilson, "Light dosimetry for intraperitoneal photodynamic therapy in a murine xenograft model of human epithelial ovarian carcinoma," *Photochem Photobiol.*, vol. 68, pp. 281–288, 1998.

[16] J. C. Lin and A. W. Guy, "A note on the optical scattering characteristics of whole blood," *IEEE Trans. Biomed. Eng.*, vol. BME-21, pp. 43–45, 1974.

[17] R. A. Meyer, "Light scattering from red blood cell ghosts: sensitivity of angular dependent structure to membrane thickness and refractive index," *Appl. Opt.*, vol. 16, pp. 2036–2038, 1977.

[18] J. R. Mourant, T. M. Johnson, G. Los, and I. J. Bigio, "Non-invasive measurement of chemotherapy drug concentrations in tissue: preliminary demonstrations of *in vivo* measurements," *Phys. Med. Biol.*, vol. 44, pp. 1397–1417, 1999.

[19] A. M. K. Nilsson, P. Alsholm, A. Karlsson, and S. Andersson-Engels, "T-matrix computations of light scattering by red blood cells," *Appl. Opt.*, vol. 37, no. 13, pp. 2735–2748, 1998.

[20] A. Taflove, *Computational Electrodynamics: The Finite-Difference Time-Domain Method*. Boston, MA: Artech House, 1995.

[21] V. I. Tatarski, *Wave Propagation in a Turbulent Medium*. New York: McGraw-Hill, 1961.

[22] S. V. Tsinopoulos and D. Polyzos, "Scattering of He-Ne laser light by an average-sized red blood cell," *Appl. Opt.*, vol. 38, no. 25, pp. 5499–5510, 1999.

[23] S. V. Tsinopoulos, E. J. Sellountos, and D. Polyzos, "Light scattering by aggregated red blood cells," *Appl. Opt.*, vol. 41, no. 7, pp. 1408–1417, 2002.

[24] P. C. Waterman, "Symmetry, unitarity, and geometry in electromagnetic scattering," *Phys. Rev. D*, vol. 3, no. 4, pp. 825–839, 1971.

[25] K. S. Yee, "Numerical solution of initial boundary value problems involving Maxwell's equations in isotropic media," *IEEE Trans. Antennas Propagat.*, vol. AP-14, pp. 302–307, May 1966.

Anders Karlsson was born in 1955, Gothenburg, Sweden. He received the M.Sc. and Ph.D. degrees, from Chalmers University of Technology, Gothenburg, Sweden, in 1979 and 1984, respectively. Since 2000 he is a Professor at the Department of Electroscience at the Lund University, Lund, Sweden.

His research activities include scattering and propagation of waves, inverse problems, and time-domain methods. Currently, he is involved in projects concerning propagation of light in blood, wireless communication with implants, and design of passive components on silicon.

Jiangping He received the B.Sc. degree in physics from Zhejiang Normal University and the Ph.D. degree in condense matter physics from Zhejiang University, Hangzhou, China, in 1995 and 2000, respectively.

From 2000–2002, he held a research position at the Department of Optical engineering, Zhejiang University, where he worked mainly on the computational electromagnetic methods for photonic crystals. From 2002–2003, he was a Visiting Scientist with the Department of Electroscience at Lund University, Lund, Sweden, where he was engaged in research project of light propagation in blood. He is now with the Department of Physics, Linkoping University, Linkoping, Sweden. His research interests include photonic crystals, electromagnetic theory, condense matter physics, and computer simulation techniques in physics and biology.

Johannes Swartling received the M.Sc. degree in engineering physics and Ph.D. degree in atomic physics from the Lund Institute of Technology, Lund, Sweden, in 1997 and 2002, respectively.

He is presently a Postdoctoral Research Scientist with the Department of Physics, Politecnico di Milano, Milan, Italy. His research interests cover spectroscopy of turbid media—especially for biomedical applications—and modeling of light propagation in scattering media.

Stefan Andersson-Engels is a Professor at Atomic Physics Division at Lund University, Lund, Sweden. His research interests are within laser spectroscopy of tissue mainly for detection, localization or delineation of diseased regions, but also for measurements of physiological properties. The clinical applications of this research could be demarcation of malignant tumours in the skin, oral, or laryngeal regions, in the urinary bladder, in the brain or in the gastrointestinal tract. Another application is detection of tissue alterations in the cardiovascular region, such as atherosclerotic plaques and a rejected organ following heart transplantation. A second major part of his research is the development and evaluation methods for laser treatments of diseases.